



## Study on the evolution of reinforced PVDF hollow fiber membrane morphology and strong hydrophobicity

Yan-Jie Wu<sup>a,b</sup>, Chang-Fa Xiao<sup>a,b,\*</sup>, Qing-Lin Huang<sup>a,b</sup>, Kai-Kai Chen<sup>a,b</sup>

<sup>a</sup>School of Textiles, Tianjin Polytechnic University, Tianjin 300387, China, email: cfxiao@tjpu.edu.cn (C.-F. Xiao); Tel. +86 22 83955299

<sup>b</sup>State Key Laboratory of Separation Membranes and Membranes Processes, Tianjin Polytechnic University, Tianjin 300387, China

Received 7 August 2017; Accepted 24 December 2017

### ABSTRACT

Reinforced polyvinylidene fluoride (PVDF) hollow fiber membranes that contained hollow braided tube and coated surface were prepared by concentric circles spinning method. The braided tube was prepared by two-dimensional braided technique using polyester (PET) filaments, while PVDF as the coated surface was obtained by nonsolvent-induced phase separation method. The effects of vapor-bath time on the structure and morphology of hollow fiber membrane were investigated, and the results could be concluded: (1) Extension of vapor-bath time would induce the roughness of coated surface which was observed by atomic force microscopy (AFM). When the vapor-bath time was 18 h, the static water contact angle reached as high as 139.2°; (2) Not only the porosity but also the mean pore size of the hollow fiber membranes was promoted as the increase of vapor-bath time. However, the liquid entrance pressure decreased obviously; (3) The characterization of membranes' cross-section morphologies disclosed that the evolution of pore's morphology switched from fingerlike to spongelike when the coagulation condition changed.

*Keywords:* Polyvinylidene fluoride (PVDF); Two-dimensional braid; Reinforced; Hollow fiber membrane; Vapor-bath

### 1. Introduction

Manufacturing of polymeric membranes is mainly based on phase separation processing. Techniques such as temperature-induced phase separation (TIPS) and nonsolvent-induced phase separation (NIPS) have been developed to produce the demixing of a homogeneous polymer solution in two phases, a polymer-rich and a polymer-lean phase [1,2]. In the TIPS process, the polymer dope solution is prepared by mixing the polymer and diluent at high temperature, followed by cooling to induce phase separation. Subsequent removal of the diluent facilitates the formation of a membrane with symmetric pores. During the NIPS process, a homogenous polymer solution is prepared by dissolving the polymer and pore-forming agents in the solvent, and then casted into a flat-sheet membrane or spun into a hollow fiber, finally immersing in a coagulation bath

(typically water or mixture of water and solvent) [3,4]. NIPS method usually leads to the formation of an asymmetric structure that composes of dense and smooth skin layer [5–7], and porous support layer with fingerlike macroporous structure [8]. However, the dense skin layer usually brings about the lower permeability. Especially, when the hydrophobic polymeric membrane is utilized in some membrane processes of membrane contactors, the smooth surface will result in the decrease of hydrophobicity. A great number of studies have been carried out to gain a better roughness structure by varying the coagulation conditions, such as water vapor, alcohol, mixtures of water with various alcohols or with various solvents, and so on [9,10]. Vapor-induced phase separation (VIPS) is classified as a kind of NIPS process. In a VIPS process, the nonsolvent sorption of vapor gas is introduced into a polymer solution which leads to the phase separation. When a low-volatility solvent is employed to prepare the membrane, the evaporation of solvent is slower than the intake of nonsolvent, resulting in a region with

\* Corresponding author.

Presented at 2017 Qingdao International Water Congress, June 27–30, 2017, Qingdao, China.

low polymer concentration near the membrane surface [11]. Widjojo et al. [12] have investigated the effects of the external and internal coagulants on the structure and morphology of polyetherimide/polyimide dual layer hollow fiber membranes. A more open-cell structure with macrovoids can be observed in the outer and inner layers when the solubility parameter differed from that of the polymer matrix. Pereira et al. [13] have reported that a longer air gap distance can prolong the contact time for the interpenetration of the outer and inner dope solutions at the interfacial region. Bonyadi et al. [14] also have observed the effect of the air gap during the fabrication of single-layer polyacrylonitrile membranes.

It is well known, according to the theory of Wenzel, that the increase of surface roughness not only improves the actual gas liquid contact area, but also strengthens the interface effect. Therefore, as the surface roughness increases, hydrophilic membrane will become more hydrophilic and hydrophobic membrane becomes more hydrophobic [15]. Many attempts of hydrophobic/hydrophilic modification by regulating the membrane morphology can be found in the past decades. Some common measures such as surface etching, coating, template method, and blending on the membrane morphology regulation have been carried out in many literatures. Sun et al. [16] have created a rough super-hydrophobic surface using a lotus leaf as template and replicated it by nanoscale casting instead of conventional microfabrication or chemical synthesis. Yan et al. [17] have combined nano-CaCO<sub>3</sub> particles with polyvinylidene fluoride (PVDF) matrix to make a coating surface highly rough and porous in microscopic scales. However, these methods suffer from the disadvantages of cumbersomeness and inefficiency. Peng et al. [18] and Peng et al. [19] have prepared porous, highly hydrophobic PVDF surfaces with micro- and nanoscale hierarchical roughness via VIPS.

In addition, the commercial hollow fiber membrane prepared by NIPS method deserves low-mechanical endurance which limits its application in engineering practice [20]. Some researches have been carried out to improve the membrane's mechanical properties [21–24]. Liu et al. [25] have prepared the polyester (PET) threads reinforced PVDF hollow fiber membranes by incorporating PET threads in the support layer of hollow fiber membrane in axial direction as a special reinforced material. Zhang et al. [26] have studied on the interfacial bonding state and fouling phenomena of PVDF matrix-reinforced hollow fiber membranes during microfiltration.

The objective of this study is providing a novel approach to fabricate a kind of reinforced hydrophobic PVDF hollow fiber membrane. The reinforced hollow fiber membranes composed of braided tubular and coated layer were fabricated

via dry-wet spinning process. The coated layer is obtained by coating the PVDF casting solutions on the outer surface of braided tubular through concentric circles spinning method. During this process, vapor-bath phase inversion method and hollow tube braided reinforced method are combined to improve membrane's hydrophobicity and mechanical strength. The effects of vapor-bath time on the membrane's performance in terms of permeability, hydrophobicity, and surface roughness are investigated.

## 2. Experimental

### 2.1. Materials

PVDF (Solef 6010) was purchased from by Solvay Co., Ltd., Belgium. PET was kindly provided by Tianjin Polytechnic University, China. *N,N*-dimethylacetamide (DMAc) (Synthesis Grade, Tianjin Kermel Chemical Reagent Co., Ltd, >99%) was employed as solvent to prepare the polymer casting solution without further purification. Lithium chloride (LiCl) (Synthesis Grade, Tianjin Kermel Chemical Reagent Co., Ltd., Tianjin) was used as inorganic additives.

### 2.2. Membrane preparation

#### 2.2.1. Dope preparation

The casting solutions were prepared by dissolving PVDF powder into preweighed DMAc solvent and then magnetically stirred for 3 h at 70°C. The PVDF, DMAc, and LiCl in a special mass ratio were mixed homogeneously under high-speed agitation, and the parameters are shown in Table 1. The prepared casting solution was kept for 3 h without stirring at 70°C to remove air bubbles.

#### 2.2.2. Fiber spinning

Fig. 1 shows the conventional two-dimensional braiding mechanism. The spindles held the bobbins and supplied the yarn. The movement of spindle intertwined the yarns so that the braided structure was formed. The braiding mechanism consisted of the take-up mechanism and the spindle movement, and the spindle movement along the circle could be regarded as one-dimensional. The formed braided hollow tube was taken up in the vertical direction, which was also a one-dimensional movement. Simple shapes such as tubular braids could be fabricated by a combination of these two-dimensional movements.

The PET filaments were braided into a braided tube by braiding machine (Xuzhou Henghui Braiding Machine Co., Ltd., Jiangsu, China). The woven pitch was 7 mm, and the

Table 1  
Formulation of the hollow fiber membrane

| Sample | Vapor-bath (h) | PVDF (wt%) | DMAc (wt%) | LiCl (wt%) | Tween 80 (wt%) | Inter diameter (mm) | Outer diameter (mm) | Coated layer thickness (mm) |
|--------|----------------|------------|------------|------------|----------------|---------------------|---------------------|-----------------------------|
| P0     | 0              | 28         | 67         | 3          | 2              | 0.50 ± 0.09         | 1.56 ± 0.07         | 0.26 ± 0.08                 |
| P1     | 6              | 28         | 67         | 3          | 2              | 0.53 ± 0.15         | 1.57 ± 0.05         | 0.28 ± 0.05                 |
| P2     | 12             | 28         | 67         | 3          | 2              | 0.52 ± 0.11         | 1.53 ± 0.03         | 0.28 ± 0.04                 |
| P3     | 18             | 28         | 67         | 3          | 2              | 0.53 ± 0.08         | 1.54 ± 0.04         | 0.27 ± 0.05                 |

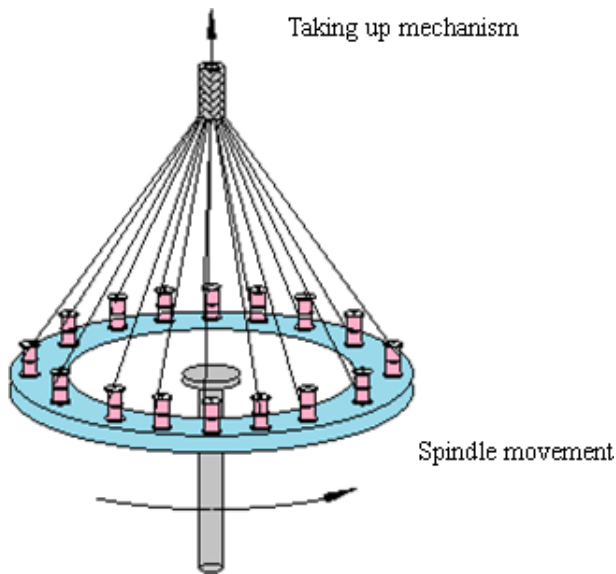


Fig. 1. The scheme of conventional two-dimensional braiding apparatus.

weaving speed was 1,823 mm/min. At room temperature, the mechanical strength of PET hollow braided tubular was approximately 100 MPa. The schematic diagram of the two-dimensional reinforced hollow tube is shown in Fig. 1. The obtained PET braided hollow tube was cleaned as to remove the oil and then dried at room temperature.

To keep the hollow fiber membrane structure, PET braided tube was used as support layer. PVDF hollow fiber membranes were spun via dry-jet wet method using the spinning system schematically as shown in Fig. 2. The prepared dope solution was loaded into the spinning dope tank while the braided tubular passed through the spinneret. Under the certain tension provided by payoff and take-up device, the hollow braided tube would locate in the center of the concentric circles spinning system which made the dope solution coated on the outer surface homogeneously and finally obtained the same thickness of separation layer (PVDF layer). The braided tube was homogeneously coated with the PVDF dope solution, after which, the deionized water or water vapor was utilized as the coagulant bath, and the hollow fiber membranes were collected and kept in deionized water for at least 3 d. The detailed parameters are summarized in Table 1. In addition, due to the high strength and flexibility of PET braided tube, the original cross-section of reinforced PVDF hollow fiber membrane was difficult to obtain by frozen in liquid  $N_2$ . The mechanical strength of PVDF reinforced hollow fiber membrane was approximately 100 MPa as shown in Fig. 3.

### 2.3. Method and measurements

#### 2.3.1. Morphology observation

The morphologies of the resulting membranes were observed using scanning electron microscopy (SEM, Quanta200, FEI, Czech Republic). The samples were freeze dried for 2 d and then were cut off using a razor blade. Samples were prepared by platinum coating.

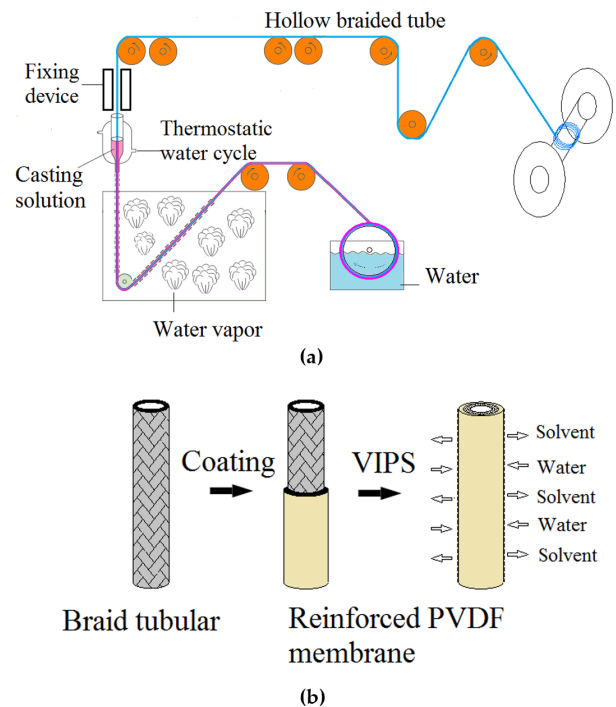


Fig. 2. The scheme of dry-jet wet spinning process: (a) preparation process of the PVDF membranes and (b) PVDF membranes.

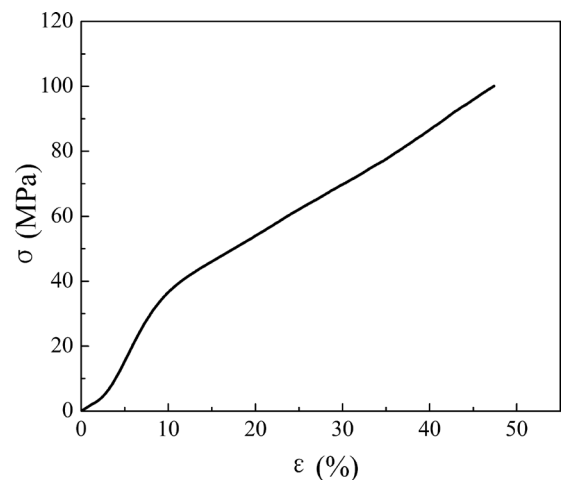


Fig. 3. The mechanical properties of PVDF reinforced hollow fiber membranes.

#### 2.3.2. Porosity

The membrane porosity was defined as the pores volume divided by the total volume of the porous membrane. It can be determined by gravimetric method [27]. It can be determined by Eq. (1) as follows:

$$\varepsilon(\%) = \frac{W_1 - W_2}{(\pi/4)(D^2 - d^2)l\sigma} \times 100\% \quad (1)$$

where  $W_1$  is the weight of the wet membrane (g),  $W_2$  is the weight of the dry membrane (g),  $\sigma$  is the butanol density

( $\rho = 0.8098 \text{ g cm}^{-3}$ ),  $D$  is the outer diameter (cm),  $d$  is the inner diameter (cm), and  $l$  is the length of sample membrane (cm).

The pore size and its distribution of the membranes were determined by using automated capillary flow porometer (CFP-1100-A, Porous Materials, Inc., USA).

### 2.3.3. Contact angle

The hydrophobicity of the obtained membranes was calculated by measurement of the water contact angle. The contact angles of all the samples were measured by an optical contact angle meter (model JYSP-180, Jinshengxin Inspection Instrument Co., Ltd., Germany). A water droplet was dropped on the sample surface. Each sample was tested five times to evaluate the average value.

### 2.3.4. Permeability tests

The reinforced PVDF hollow fiber membranes were characterized by using carbon ink solution. The ink solution flux of the membranes was measured with a 0.5 ng/L ink solution. The particle distribution of the ink solution is shown in Fig. 4. The pressure difference across the membrane was 0.1 MPa. The flux was calculated by Eq. (2) as follows:

$$J_l = \frac{V}{A \times t} \quad (2)$$

where  $J_l$  is the permeation flux ( $\text{L} \cdot \text{m}^{-2} \cdot \text{h}^{-1}$ ),  $V$  is the total permeation (L),  $A$  is the membrane area ( $\text{m}^2$ ), and  $t$  is the sampling time (h).

The concentration of feed solution and permeate solution was determined by UV spectroscopy at wavelength of 644 nm, using a Shimadzu UV-2450 spectrophotometer. The separation efficiency of the membrane was defined by the following equation:

$$R = (1 - C_p / C_f) \times 100\% \quad (3)$$

where  $R$  is the rejection (%),  $C_f$  and  $C_p$  are the concentrations of the ink in the feed and the permeate solution, respectively.

Gas permeation flux of dry membrane was determined by Eq. (4). The permeate flow rate was measured at different pressures as shown in Fig. 5. The lumen side of each membrane module was connected to a nitrogen cylinder. The permeation flux of nitrogen through the dried membranes was measured at room temperature.

$$J_g = \frac{L}{A} \quad (4)$$

where  $J_g$  is the nitrogen flux ( $\text{m}^3 \cdot \text{m}^{-2} \cdot \text{h}^{-1}$ ),  $L$  is the nitrogen flow ( $\text{m}^3 \cdot \text{h}^{-1}$ ), and  $A$  is the membrane area ( $\text{m}^2$ ).

Liquid entrance pressure (LEP) of dry membrane was accessed using laboratory-made device at room temperature as shown in Fig. 6. This pressure depended on the pore size and the hydrophobicity of the membrane. The pressure increased slowly until the mutation of conductivity meter. This mutation pressure was considered as the LEP point. The

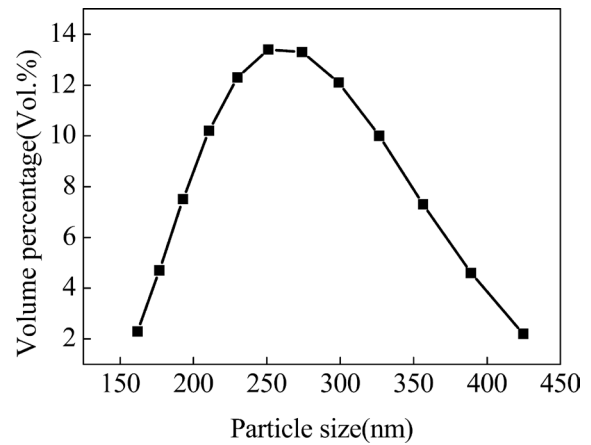


Fig. 4. The particle distribution of the ink solution.

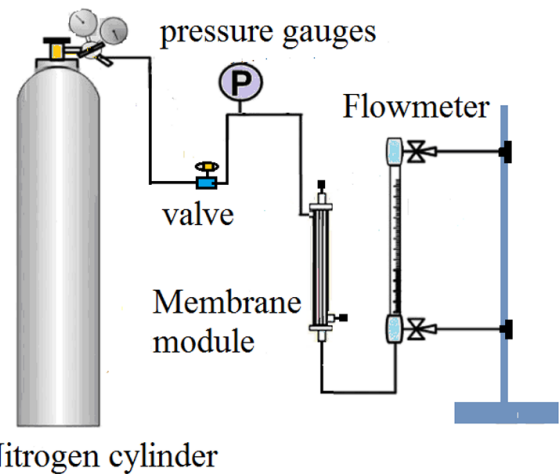


Fig. 5. Gas permeation flux of the hollow fiber membrane testing device.

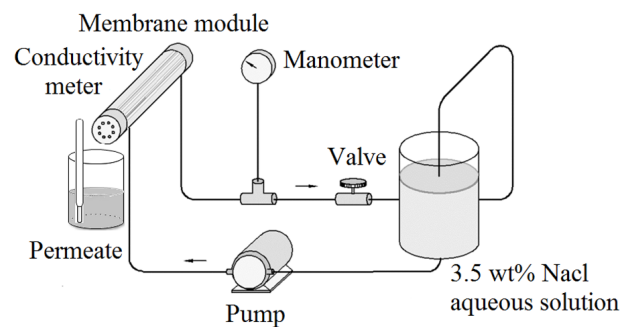


Fig. 6. LEP of the hollow fiber membrane testing device.

LEP of membrane was tested for three times to evaluate the average value.

### 2.3.5. Roughness

Membrane surfaces' roughness and stereo morphology were observed by atomic force microscopy (AFM, 5500, Agilent Company, USA).

### 3. Result and discussion

#### 3.1. Effect of the vapor-bath times on membrane porosity and permeability

The effects of the vapor-bath time on permeation flux and rejection are shown in Fig. 7. It was observed that the permeation flux increased obviously when vapor bath was utilized as the coagulation, and the rejection presented the opposite trend. As for P0 membrane, this trend was probably due to the fact that water was a strong nonsolvent that induced a rapid coagulation in the nascent membrane surface and consequently led to the formation of a dense skin with a low surface porosity (as shown in Fig. 8). Therefore, P0 deserved a lowest permeation flux while the rejection was the highest. When vapor bath was utilized as coagulant, the coagulation speed became much slow thereby inducing the disappearance of dense skin layer and the appearance of the open-cell macrovoids. Moreover, as the vapor-bath time increasing, the formation of open-cell macrovoids became more complete which brought about the improvement of porosity and  $N_2$  flux. LEP and  $N_2$  flux results agreed well with the change of the porosity presented in Fig. 9. The maximum  $N_2$  flux reached as high as  $10 \text{ m}^3 \cdot \text{m}^{-2} \cdot \text{h}^{-1}$  when the vapor-bath time was 12 h.

Fig. 10 showed the effect of vapor-bath time on the pore size and distribution of reinforced PVDF hollow fiber membranes. It could be clearly seen that P0 membrane exhibited a narrower pore size distribution than P1, P2, and P3 membrane, and the maximum pore size and mean pore size of the braided reinforced membranes became bigger with the increase of vapor-bath time. The results agreed with the flux and porosity very well.

#### 3.2. Effects of the vapor-bath time on membrane morphology

Fig. 11 shows the SEM pictures of the outer surface of the braided tube reinforced PVDF hollow fiber membranes with different vapor-bath times. It could be clearly observed that P0 membrane had a dense and smooth surface with no obvious pores (Fig. 11(a)). However, when the water vapor was introduced as the coagulant bath, the roughness of the membrane surface increased considerably. It could be seen that the number and the size of the surface pores increase with the increase of the vapor-bath time. The reasons could be concluded as follows: (1) compared with the water-inversion method, VIPS (water vapor) diffused into the casting membrane with a much slower rate because that the process introduced a gas phase mass transfer resistance to the membrane formation system; (2) when a low-volatility solvent was employed as the polymer solvent, the evaporation of solvent was slower than the intake of nonsolvent, resulting in a region with low polymer concentration near the membrane surface.

The water contact angles of the obtained membranes were measured and the average values rose from  $91.9^\circ$  to  $139.2^\circ$  as the increase of vapor bath time. According to the theory of Wenzel, the higher surface roughness of membrane would induce the stronger hydrophobicity. The results of water contact angle with different vapor-bath time agreed well with the corresponding SEM pictures shown in Fig. 11.

Due to the difficulty of fracture in liquid  $N_2$ , the braided reinforced hollow fiber membrane was cut off using a razor

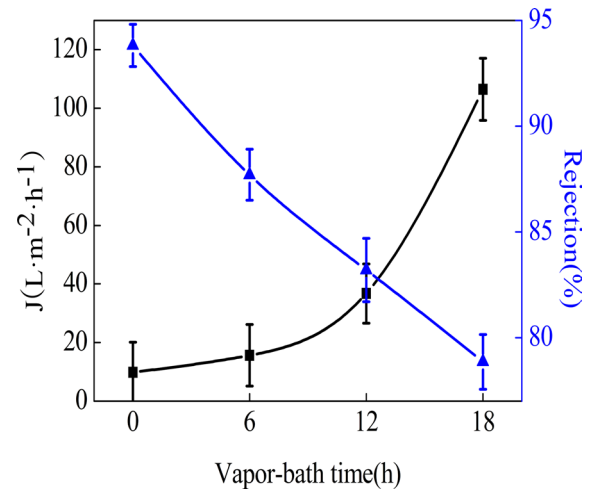


Fig. 7. Effect of the vapor-bath time on permeation flux and rejection.

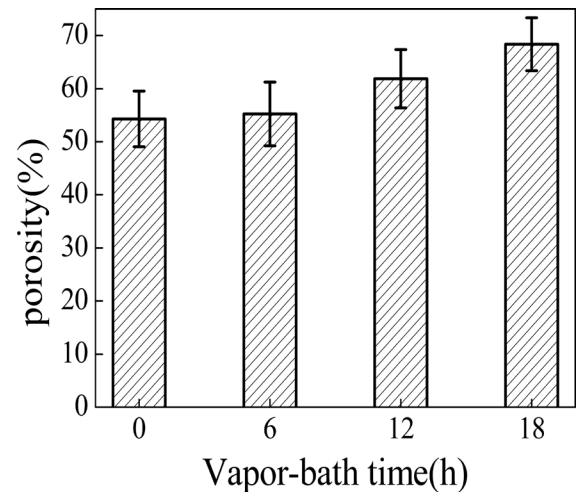


Fig. 8. Effect of the vapor-bath time on porosity.

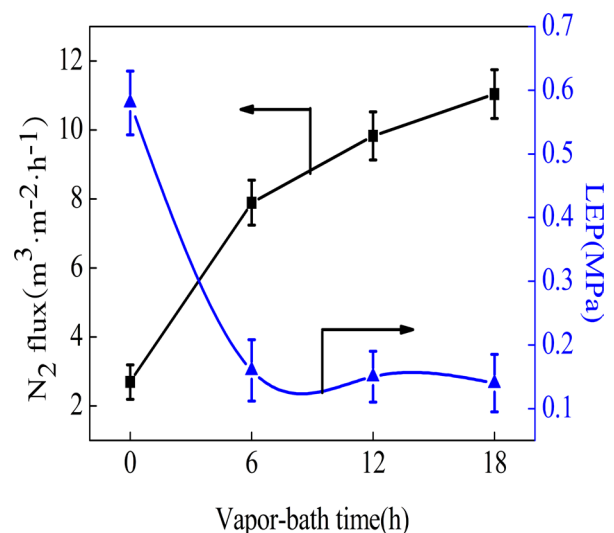


Fig. 9. Effect of the vapor-bath time on  $N_2$  flux and LEP.

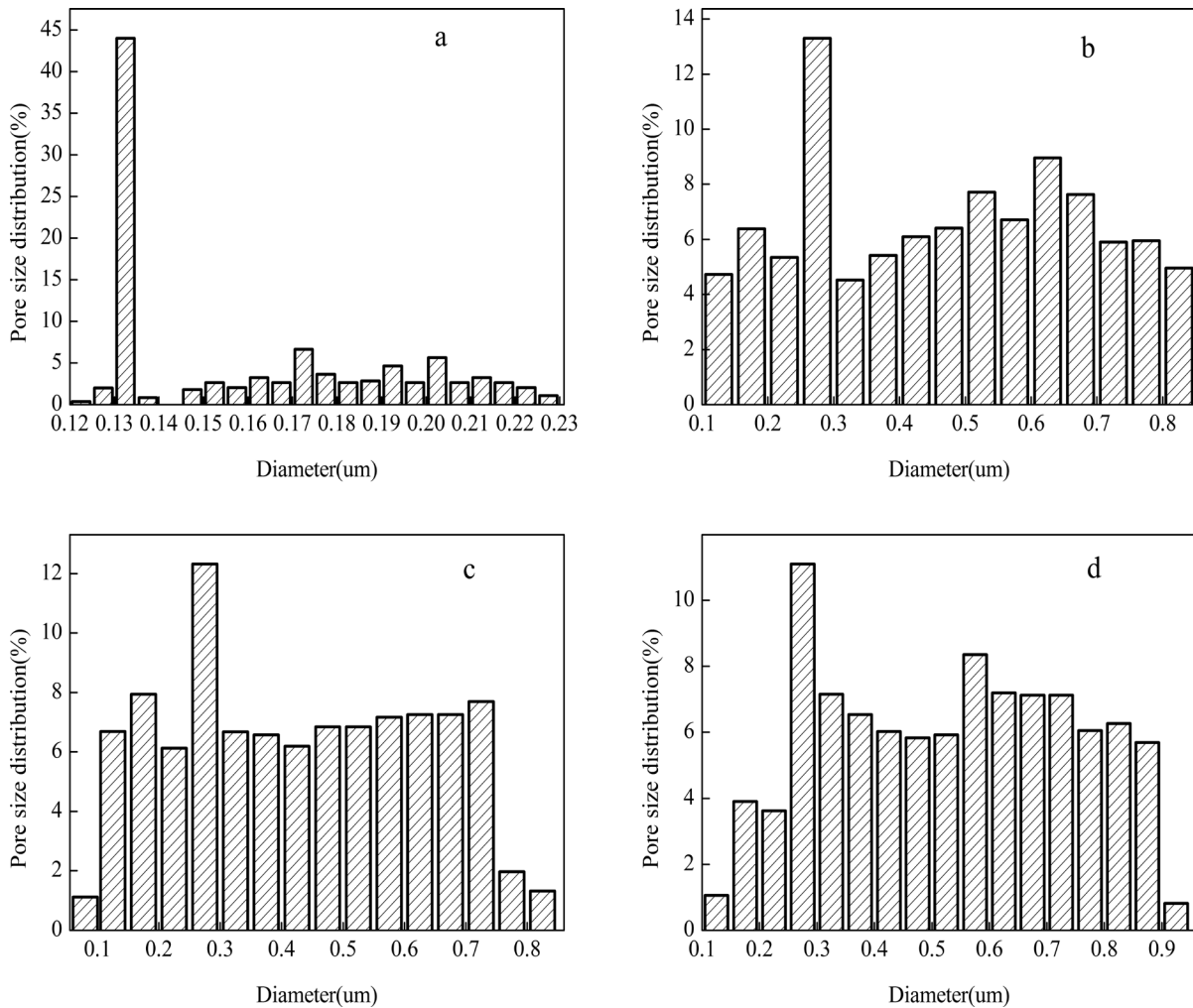


Fig. 10. Pore size and distribution of braided reinforced PVDF hollow fiber membranes: (a) P0, (b) P1, (c) P2, and (d) P3.

blade to expose its cross-sectional area, and the cross-section morphology of separation surface was destroyed by the razor blade which is shown in Fig 12. It could be found that P0 membrane exhibited an asymmetric structure with dense skin layer and a fingerlike pore structure supported by a spongelike structure. A uniform spongelike structure extended over the membrane cross-section. However, the dense skin layer disappeared gradually when water vapor was used as an external coagulant. As the vapor-bath time increasing, the membrane structure changed from fingerlike to spongelike. As water was a kind of strong nonsolvent, it induced fast coagulation when the casting solution immersed into water. The fast coagulation would result in the formation of dense skin layer and the fingerlike pore structure. When the vapor bath was utilized as the coagulation, the slow coagulant rate resulted in the disappearance of dense skin layer and spongelike pore structure.

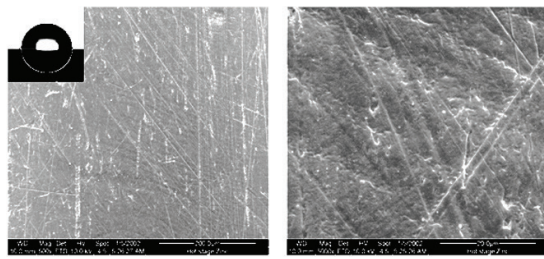
### 3.3. Effect of the vapor-bath time on membrane surface roughness

Three-dimensional AFM pictures of PVDF membranes' outer surface with different vapor-bath times are presented in Fig. 13. As expected, an obvious difference in the morphology

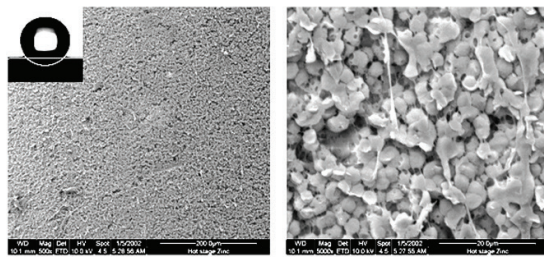
could be observed. The images were presented in small scanning area with Z range, which revealed the surfaces roughness of membranes. The surface morphology of P0 membrane was much different from the one of water vapor coagulation (P1, P2, and P3). Moreover, as the vapor-bath time increasing, the roughness parameters Ra which represented the surface roughness increased from 0.832 to 1.811 (Table 2). The results were attributed to the presence of open-cell structure with macrovoids.

## 4. Conclusions

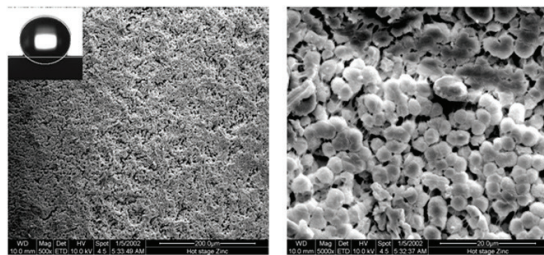
Braided tube reinforced PVDF hollow fiber membranes with different pore structure were prepared by concentric circles spinning method. The effects of vapor-bath time on the membranes' surface and the performances of reinforced PVDF hollow fibers membrane were investigated, respectively. The extension of vapor-bath time induced the increase of outer surface's roughness. The porosity and permeation flux of the PVDF membrane promoted obviously while the LEP and the rejection decreased as vapor-bath times increasing. The SEM pictures of membranes' cross-section revealed that fingerlike structure were formed when water was used



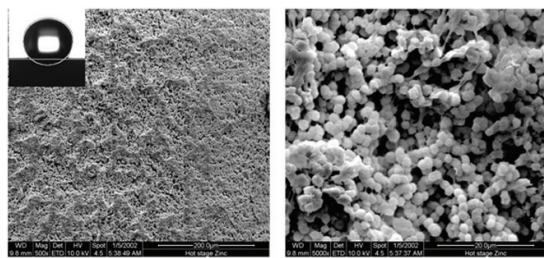
(a)  $91.9^\circ \pm 0.34$



(b)  $135^\circ \pm 0.10$



(c)  $135.5^\circ \pm 0.09$



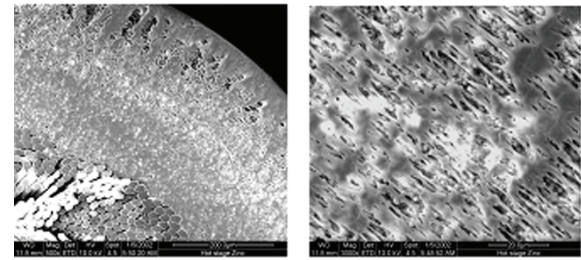
(d)  $139.2^\circ \pm 0.16$

Fig. 11. SEM images and water contact angles of the PVDF membranes with difference vapor-bath times: (a) P0 ( $91.9^\circ \pm 0.34$ ), (b) P1 ( $135^\circ \pm 0.10$ ), (c) P2 ( $135.5^\circ \pm 0.09$ ), and (d) P3 ( $139.2^\circ \pm 0.16$ ) (left,  $\times 500$ ; right,  $\times 5000$ ).

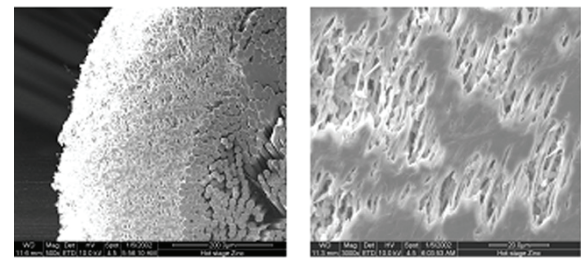
as coagulant, whereas a spongelike structure gradually appeared when water vapor was used.

**Acknowledgments**

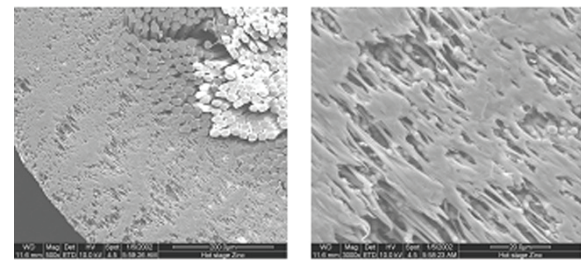
This work was supported by Tianjin Key Research Program of Application Foundation and Advanced Technology (No. 12JCZDJC26600) and Tianjin Platform Construction Plan for Science and Technology Innovation System (13TXSYJC40300).



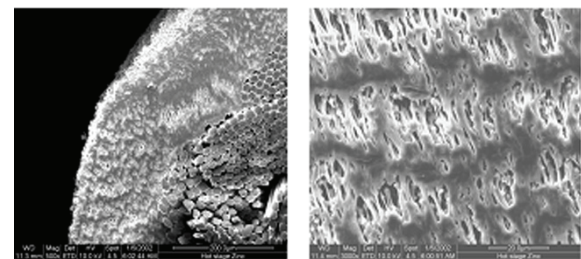
(a)



(b)



(c)



(d)

Fig. 12. SEM images of the PVDF membrane with difference vapor-bath times: (a) P0, (b) P1, (c) P2, and (d) P3 (left,  $\times 500$ ; right,  $\times 3000$ ).

**List of symbols**

|               |   |                                |
|---------------|---|--------------------------------|
| $\varepsilon$ | — | Porosity                       |
| $W_1$         | — | Weight of the wet membrane (g) |
| $W_2$         | — | Weight of the dry membrane (g) |
| $D$           | — | Outer diameter (cm)            |
| $d$           | — | Inner diameter (cm)            |
| $l$           | — | Length of sample membrane (cm) |

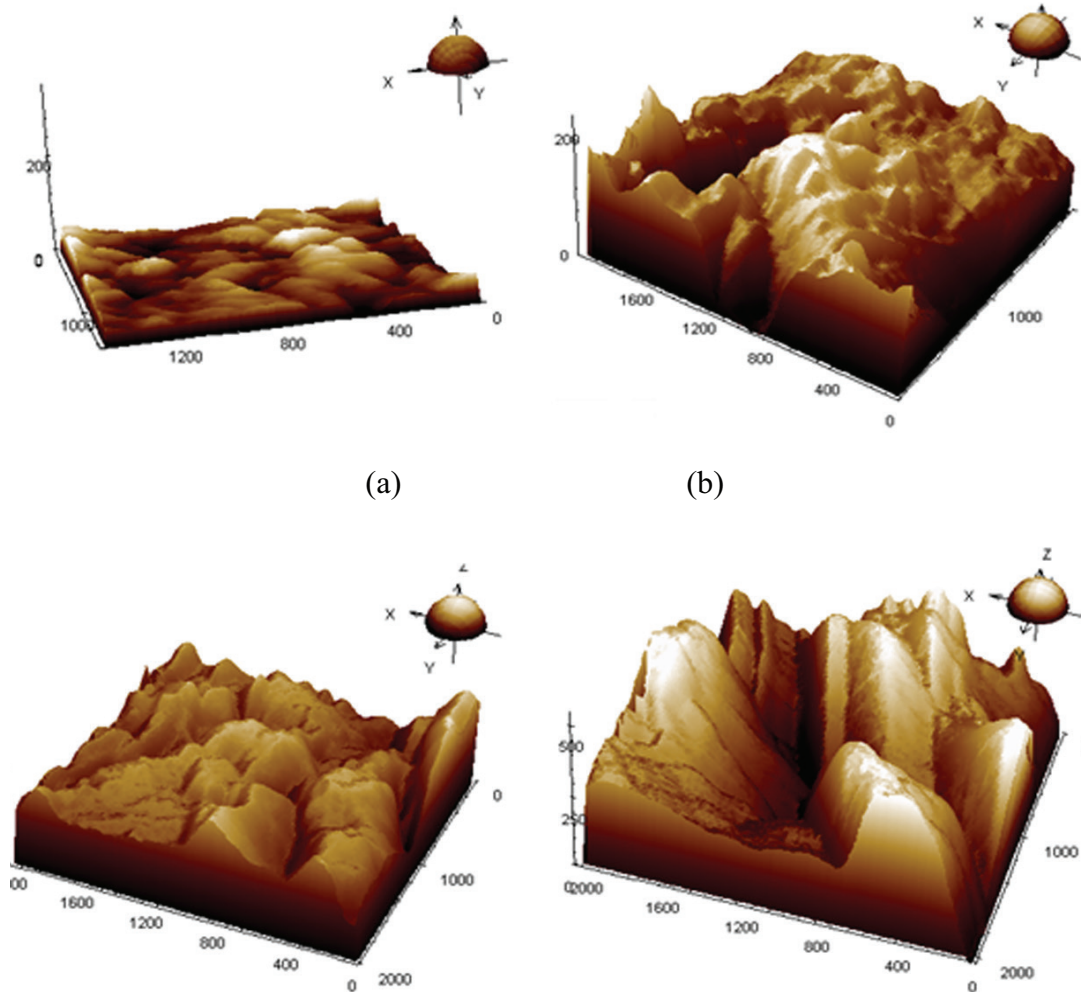


Fig. 13. AFM images of the PVDF membrane’s surface with difference vapor-bath times: (a) P0, (b) P1, (c) P2, and (d) P3.

Table 2  
Roughness of the PVDF membranes by difference vapor-bath times

| Vapor-bath time (h) | Ra ( $\mu\text{m}$ ) |
|---------------------|----------------------|
| 0                   | 0.832                |
| 6                   | 1.218                |
| 12                  | 1.475                |
| 18                  | 1.811                |

|          |   |  |
|----------|---|--|
| $\sigma$ | — | Water density ( $\text{kg m}^{-3}$ )                       |
| $J_l$    | — | Permeation flux ( $\text{L m}^{-2} \text{h}^{-1}$ )        |
| $V$      | — | Total permeation (L)                                       |
| $A$      | — | Total permeation area ( $\text{m}^2$ )                     |
| $t$      | — | Total permeation time (h)                                  |
| $R$      | — | Rejection (%)  |
| $C_p$    | — | Concentration of the ink in the feed                       |
| $C_f$    | — | Concentration of the permeate solution                     |
| $J_g$    | — | Nitrogen flux ( $\text{m}^3 \text{m}^{-2} \text{h}^{-1}$ ) |
| $L$      | — | Nitrogen flow ( $\text{m}^3 \text{h}^{-1}$ )               |

### References

- [1] M. Di Luccio, R. Nobrega, C.P. Borges, Microporous anisotropic phase inversion membranes from bisphenol-A polycarbonate: study of a ternary system, *Polymer*, 41 (2000) 4309–4315.
- [2] C.-Y. Kuo, H.-N. Lin, H.-A. Tsai, D.-M. Wang, J.-Y. Lai, Fabrication of a high hydrophobic PVDF membrane via nonsolvent induced phase separation, *Desalination*, 233 (2008) 40–47.
- [3] J.H. Kim, B.R. Min, J. Won, H.C. Park, Y.S. Kang, Phase behavior and mechanism of membrane formation for polyimide/DMSO/water system, *J. Membr. Sci.*, 187 (2001) 47–55.
- [4] P.S.T. Machado, A.C. Habert, C.P. Borges, Membrane formation mechanism based on precipitation kinetics and membrane morphology: flat and hollow fiber polysulfone membranes, *J. Membr. Sci.*, 155 (1999) 171–183.
- [5] D. Wang, K. Li, W.K. Teo, Preparation and characterization of polyvinylidene fluoride (PVDF) hollow fiber membranes, *J. Membr. Sci.*, 163 (1999) 211–220.
- [6] M. Khayet, C. Feng, K.C. Khulbe, T. Matsuura, Preparation and characterization of polyvinylidene fluoride hollow fiber membranes for ultrafiltration, *Polymer*, 43 (2002) 3879–3890.
- [7] M. Mulder, *Basic Principles of Membrane Technology*, Kluwer Academic Publishers, Dordrecht, 1991.
- [8] C.A. Smolders, A.J. Reuvers, R.M. Boom, I.M. Wienk, Microstructures in phase-inversion membranes. Part 1. Formation of macrovoids, *J. Membr. Sci.*, 73 (1992) 259–275.

- [9] L. Yilmaz, A.J. McHugh, Analysis of non-solvent-solvent-polymer phase diagrams and their relevance to membrane formation modeling, *J. Appl. Polym. Sci.*, 31 (1986) 997.
- [10] K. Kimmerle, H. Strathmann, Analysis of the structure-determining process of phase inversion membranes, *Desalination*, 79 (1990) 283–302.
- [11] Y.S. Su, C.Y. Kuo, D.M. Wang, J.Y. Lai, A. Deratani, C. Pochat, D. Bouyer, Interplay of mass transfer, phase separation, and membrane morphology in vapor induced phase separation, *J. Membr. Sci.*, 338 (2009) 17–28.
- [12] N. Widjojo, T.S. Chung, W.B. Krantz, A morphological and structural study of Ultem/P84 copolyimide dual-layer hollow fiber membranes with delamination-free morphology, *J. Membr. Sci.*, 294 (2007) 132–146.
- [13] C.C. Pereira, R. Nobrega, K.V. Peinemann, C.P. Borges, Hollow fiber membranes obtained by simultaneous spinning of two polymer solutions: a morphological study, *J. Membr. Sci.*, 226 (2003) 35–50.
- [14] S. Bonyadi, T.S. Chung, W.B. Krantz, Investigation of corrugation phenomenon in the inner contour of hollow fibers during the non-solvent induced phase-separation process, *J. Membr. Sci.*, 299 (2007) 200–210.
- [15] X.F. Li, C. Zhou, R.H. Du, N.N. Li, X.T. Han, Y.F. Zhang, S.L. An, C.F. Xiao, Evolution of polyvinylidene fluoride (PVDF) hierarchical morphology during slow gelation process and its superhydrophobicity, *ACS Appl. Mater. Interfaces*, 5 (2013) 5430–5435.
- [16] M.H. Sun, C.X. Luo, L.P. Xu, H. Ji, O.Y. Qi, D.P. Yu, Y. Chen, Artificial lotus leaf by nano-casting, *Langmuir*, 21 (2005) 8978–8981.
- [17] L.L. Yan, K. Wang, L. Ye, Super hydrophobic property of PVDF/CaCO<sub>3</sub> nanocomposite coatings, *J. Mater. Sci.*, 22 (2003) 1713–1717.
- [18] M. Peng, H. Li, L. Wu, Q. Zheng, Y. Chen, W. Gu, Porous poly(vinylidene fluoride) membrane with highly hydrophobic surface, *J. Appl. Polym. Sci.*, 98 (2005) 1358–1363.
- [19] Y. Peng, H. Fan, Y. Dong, Y. Song, H. Han, Effects of exposure time on variations in the structure and hydrophobicity of polyvinylidene fluoride membranes prepared via vapor-induced phase separation, *Appl. Surf. Sci.*, 258 (2012) 7872–7881.
- [20] J. Liu, P. Li, Y. Li, L. Xie, S. Wang, Z. Wang, Preparation of PET threads reinforced PVDF hollow fiber membrane, *Desalination*, 249 (2009) 453–457.
- [21] H. Fujuki, H. Habara, T. Hirane, et al., Porous Membrane, US20020046970, 2002-04-25.
- [22] Zenon Environmental INC, Hollow Fiber Membrane and Braided Tubular Support there for, US6354444.1999-06-17.
- [23] T. Eguchi, Manufacture of Porous Polysulfone Hollow Fiber Membrane Having High Strength, JP4260424.1992-09-16.
- [24] Mimubishi Rayon Co. Ltd., Composite Porous Membrane and Method for Producing the Same, US7306105.2005-05-10.
- [25] J. Liu, P. Li, Y. Li, L. Xie, S. Wang, Z. Wang, Preparation of PET threads reinforced PVDF hollow fiber membrane, *Desalination*, 249 (2009) 453–457.
- [26] X. Zhang, C. Xiao, X. Hu, X. Jin, Q. Bai, Study on the interfacial bonding state and fouling phenomena of polyvinylidene fluoride matrix-reinforced hollow fiber membranes during microfiltration, *Desalination*, 330 (2013) 49–60.
- [27] H. Matsuyama, M. Teramoto, S. Kundari, Y. Kitamura, Effect of diluents on membrane formation via thermally induced phase separation, *J. Appl. Polym. Sci.*, 82 (2001) 169–177.